Research Article

Latifa Ladel, Mohamed Mastere, Shuraik Kader, Velibor Spalević, and Branislav Dudic*

Machine learning methods for landslide mapping studies: A comparative study of SVM and RF algorithms in the Oued Aoulai watershed (Morocco)

https://doi.org/10.1515/geo-2022-0740 received May 03, 2024; accepted November 16, 2024

Abstract: Effective management of watershed risks and landslides necessitates comprehensive landslide susceptibility mapping. Support vector machine (SVM) and random forest (RF) machine learning models were used to map the landslide susceptibility in Morocco's Taounate Province. Detailed landslide inventory maps were generated based on aerial pictures, field research, and geotechnical survey reports. Factor correlation analysis carefully eliminated redundant factors from the original 14 landslide triggering factors. As a result, 30% of the sites were randomly chosen for testing, whereas 70% of the landslide locations were randomly picked for model training. The RF model achieved an area under the curve (AUC) of 94.7%, categorizing 30.07% of the region as low susceptibility, while the SVM model reached an AUC of 80.65%, indicating high sensitivity in 53.5% of the locations. These results provide crucial information for

local authorities, supporting sound catchment planning and development strategies.

Keywords: management, landslide susceptibility, machine learning models, factor correlation analysis, area under the curve, Morocco

1 Introduction

Landslides are one of the world's natural geohazards. They change the terrain and disrupt people's lives and communities wherever they occur [1–3]. The severity of climate change, unexpected construction projects, and recent global economic expansion have all intensified the social repercussions of landslides [4,5]. Statistical analysis by the Disaster Epidemiology Research Center shows that more than 17% of the natural disaster deaths are caused by landslides and other mass movements [6,7]. In northern Morocco, landslides are among the most prevalent natural disasters following floods and droughts, which are regarded as the most serious danger to the country's socioeconomic growth [8,9].

While traditional methods of landslide susceptibility mapping (LSM) have provided valuable insights, they often rely heavily on expert knowledge and can be limited by data availability. Recent studies employing machine learning (ML) techniques, such as random forest (RF) and support vector machine (SVM), have shown promise in improving the accuracy and handling complex datasets. However, there remains a lack of comparative analyses that assess the performance of these models in specific regions with diverse geological characteristics. This study aims to address this gap by evaluating the effectiveness of SVM and RF models in mapping landslide susceptibility in the Oued Aoulai watershed, highlighting their respective advantages and limitations.

The early warning system effectively mitigates the risk of catastrophic landslides, encompassing both spatial and

Latifa Ladel: Geophysics and Natural Hazards Laboratory, Department of Geomorphology and Geomatics, Scientific Institute, Mohammed V University in Rabat, Avenue Ibn Batouta, Agdal, PO Box 703, 10106, Rabat-City, Morocco, e-mail: latifa2005a@yahoo.fr

Mohamed Mastere: Geophysics and Natural Hazards Laboratory, Department of Geomorphology and Geomatics, Scientific Institute, Mohammed V University in Rabat, Avenue Ibn Batouta, Agdal, PO Box 703, 10106, Rabat-City, Morocco, e-mail: mohamed.mastere@gmail.com Shuraik Kader: School of Engineering and Built Environment, Griffith University, Nathan, QLD 4111, Australia, e-mail: shuraik10@gmail.com, shuraik.mohamedabdulkader@griffithuni.edu.au, s.mohamedabdulkader@griffirth.edu.au

Velibor Spalević: Biotechnical Faculty, University of Montenegro, Podgorica, 81000, Montenegro, e-mail: velibor.spalevic@gmail.com ORCID: Latifa Ladel 0009-0004-3032-971X; Mohamed Mastere 0000-0002-5797-1962; Shuraik Kader 0000-0002-2907-5327; Velibor Spalević 0000-0002-7800-2909; Branislav Dudic 0000-0002-4647-6026

^{*} Corresponding author: Branislav Dudic, Faculty of Management, Comenius University Bratislava, Bratislava, 81499, Slovakia; Faculty of Economics and Engineering Management, University Business Academy, 21000, Novi Sad, Serbia, e-mail: branislav.dudic@fm.uniba.sk

temporal failures [10–12]. As a result, numerous landslide prediction approaches have gained prominence in recent years, focusing on LSM methods, among others [13,14]. (i) Deterministic methods, which include "expert knowledge-based methods" and geomorphologic mapping. These methods rely on the expertise of geologists, geomorphologists, and other experts to assess site vulnerability based on field observations and existing knowledge [15]. (ii) Statistical tools include logistic regression (LR), weight of evidence, and frequency ratio (FR) [16,17]. (iii) Artificial intelligence and ML include techniques such as decision tree (DT), SVM, and artificial neural network [18–20].

The models were validated using a separate dataset that included both historical landslide occurrences and environmental factors relevant to the study area. The RF model achieved an area under the curve (AUC) value of 94.7%, while the SVM model reached an AUC of 80.65%. This validation dataset was composed of 30% of the total landslide inventory, ensuring a robust evaluation of model performance.

ML methods offer a more effective approach to LSM compared to traditional expert opinion-based and analytical methodologies due to their ability to process large datasets and identify complex patterns [21–23]. Comprehending the mechanism of landslides is necessary in order to appropriately implement LSM. After that, one must look at the connection between causative variables and landslide occurrence [24].

Despite the growing use of ML models in LSM, there remains a lack of comparative studies that systematically evaluate the performance of different algorithms in specific geographic contexts, such as the Oued Aoulai watershed in Morocco. This study aims to fill this gap by not only comparing the efficacy of SVM and RF models but also by assessing their contributions to effective risk-reduction strategies based on local geological and environmental conditions.

This research aims to evaluate the use of prediction rate and FR models in determining the landslide risk of the Oued Aoulai watershed in Taounate Province, Morocco. The research objective is to assess the benefits and drawbacks of these models as well as their ability to provide efficient risk-reduction techniques. This study employs SVM and RF models due to their complementary strengths in handling LSM. SVM is selected for its effectiveness in high-dimensional spaces, where it can accurately classify and predict landslide occurrences by identifying optimal decision boundaries. Conversely, RF is chosen for its robustness and ability to aggregate multiple DTs, which enhances the predictive accuracy and reduces the likelihood of overfitting. Together, these models provide a comprehensive approach to analyzing landslide susceptibility in the Oued

Aoulai watershed. There have been many landslides in the study area in the past. To the best of our knowledge, state-of-the-art technologies have been integrated into this research together with a thorough evaluation of the available scientific literature. The next step is to make systematic geographical links between certain characteristics and landslide episodes. Performance curves and matrices were used to evaluate the accuracy of RF and SVM models.

2 Methods

In this study, factors influencing landslide susceptibility were selected based on expert judgment and a thorough review of relevant literature, resulting in an initial list of 14 potential triggering factors. When they are selected one by one using the slope unit as the base unit, the RF and SVM models yield different ratios of the susceptibility map. A factor correlation analysis was conducted to identify multicollinearity among these factors, leading to the elimination of two redundant variables. Additionally, a sensitivity analysis was performed to assess the contribution of each factor to landslide occurrences, enabling us to prioritize the most significant variables for modeling. Figure 1 depicts the flowchart of this study, describing the essential steps involved in developing the landslide status factor, inventory, and comparison, in addition to applying different ratios and models. These methods ensured a robust selection of factors for the study area, enhancing the reliability of the susceptibility maps.

2.1 Study area

The Oued Aoulai catchment located in the Taounate Province is a sub-catchment of the Oued Ouergha catchment. It divides the Taounate Province into northern and southern parts and represents the case study for this research. In the northern part of Taounate, between latitudes 34°48′39.60″N and 34°33″ 16.77″N and longitudes 4°56′20.63Ē and 4°58′11.20Ē, the Oued Aoulai catchment is located in a region (Figure 2) with an area of 370 km², a length of 27 km, and a width of 19 km and controlled by the Ghafsay and Ratba weather stations. It is home to a diverse population around 91,900, whose livelihoods depend heavily on agriculture and natural resources. The region has experienced numerous landslides, which pose significant risks to local communities by damaging the infrastructure, disrupting the transportation networks, and affecting the agricultural productivity [25,26]. Previous

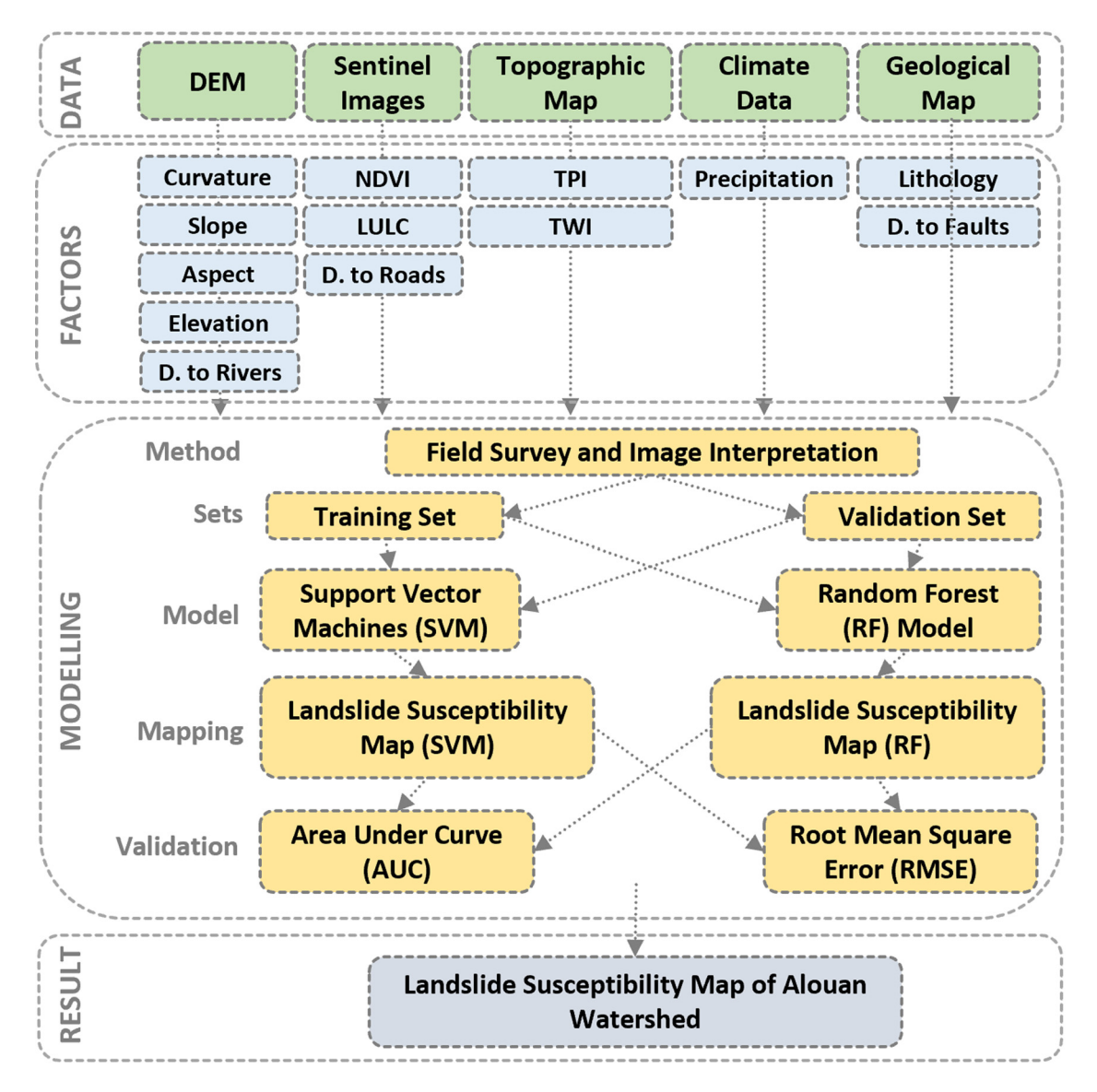


Figure 1: Flowchart of the research methodology.

research studies in the region indicate that landslides have not only led to economic losses but also threatened the safety and well-being of residents [27,28]. Given this context, effective LSM becomes crucial for informing risk management strategies and enhancing community resilience.

Part of the western Mediterranean's Alpine chain is the Rif chain, which is located in northern Morocco and is distinguished by its intricate geology. Its present structure was determined by the movement of internal zones toward the WSW and by the African and European NS convergence during the Neogene [29,30]. It consists of three major structural areas, such as inner areas, flysch zones, and outer areas, from which ancient furrows and folds are derived from north to south.

The research region is a part of the Mesorifan zone in the middle Rif area, which is made up of Neogene basins (Rhafsai, Tafrant, Taounate Bouhadi, and Dhar Souk), all of which have a synclinal structure framed by NE–SW, EW, NW accidents—SE [31]. The whole outline is an arc with a concavity-directed NE. The Aoulai watershed is part of the Tafrant—Rhafsai synclinal basin formed from Triassic to Quaternary rocks.

The facies are composed of Jurassic limestone, marl limestone, marl, thick Cretaceous marl, and marl limestone; the Tertiary cover began in the Eocene (white marl containing chert rock), then the Lower Miocene (alternating marl and sandy limestone) and the Upper Miocene, consisting of blue marl and marl sandstone.

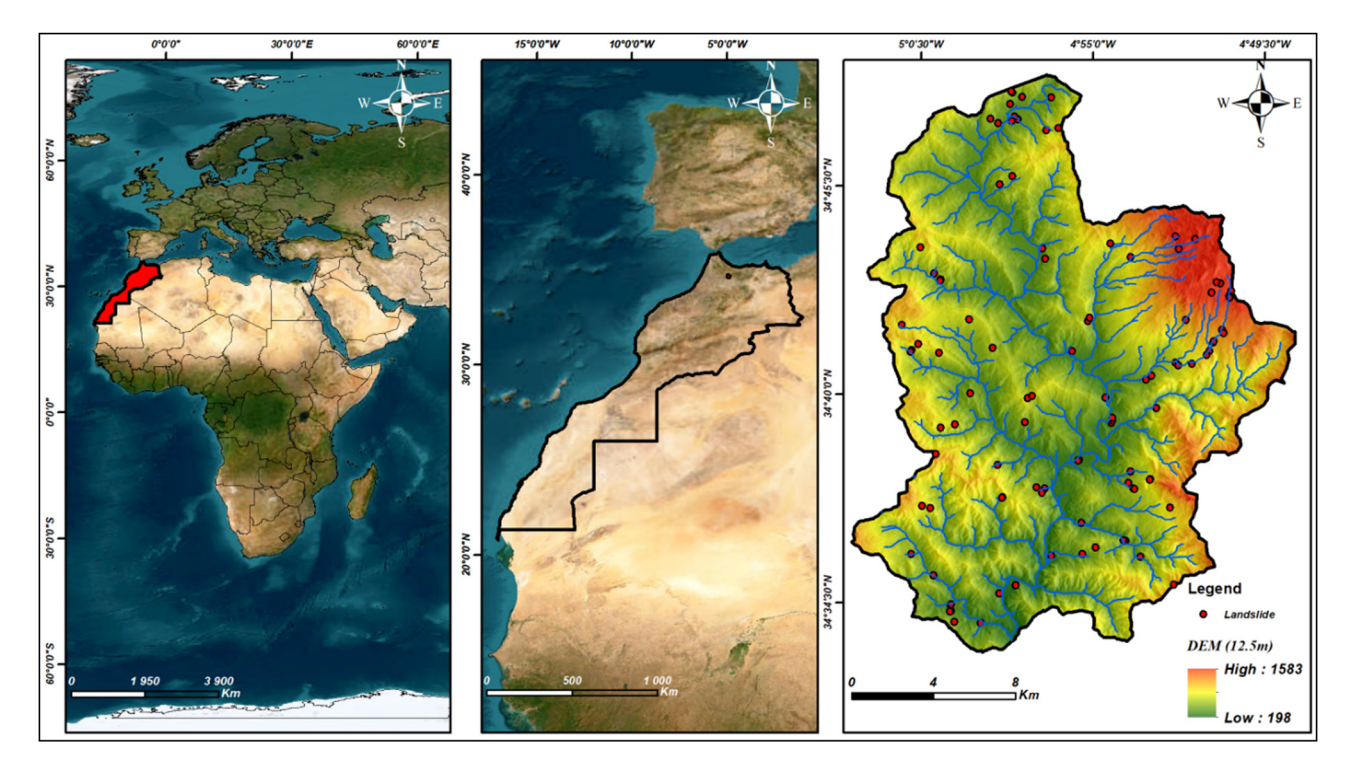


Figure 2: Geographic setting of the research area.

Quaternary is prominent and widespread in terraces or dispersed parts of the basin.

2.2 Application of various ratios and models

2.2.1 RF model

Several independent DTs that are all capable of producing results make up the RF model [32]. Based on DTs, the RF model is a categorization approach [33]. Data scientists frequently utilize the supervised learning method RF. Every DT starts with a randomly chosen sample, uses it for training, and then replaces it with the original data [34]. The RF model consists of multiple DTs that are trained independently using a method known as bootstrap aggregating or bagging. In this process, each tree is constructed using a random subset of the training data, generated by sampling with replacement. This means that some observations may be used multiple times in a single tree, while others may not be included at all. By averaging the predictions from all the DTs, the RF model reduces the variance associated with individual trees, thus minimizing the risk of overfitting to the training data. This ensemble approach enhances the model's generalization capability on unseen data. It is a reliable model that combines the outputs of several DTs into a single result and may be applied to regression and classification applications. Since the RF selection of each split node depends on two data objects – out-of-bag (OOB) and neighbor – RF is known for its high accuracy in predicting outliers [35]. When these DTs are combined, the result is the RF. In terms of outcome, this is how the RF performs better than the DT model (equation (1)).

$$H(X) = av_k \max_{i=1}^{k} I(h_i(X) = Y),$$
 (1)

where av_k shows the average, and the indicator function is denoted by I.

The RF model has many advantages, such as (i) determining correlations between variables without generating any central hypotheses [36], (ii) being a better ML program for assessing hierarchical situations in big data [36], and (iii) ranking the independent variables according to importance [37]. This approach also has the advantage of meticulously eliminating the problem of overfitting the data by (i) building multiple trees, (ii) bootstrapping observations, and (iii) dividing the nodes into optimal divisions within a randomized subset [38].

2.2.2 SVM model

The SVM family of automatic learning algorithms addresses issues with anomaly detection, regression, and classification. Vapnik was the one who first suggested the SVM for

regression [39]. In a high-dimensional or infinite space, the SVM generates a single hyperplane or a group of hyperplanes. It is applicable to both regression and classification.

Their foundation lies in the quest for the ideal marginal hypersurface that, to the greatest extent feasible, distinguishes or categorizes the data while remaining as remote from every observation as feasible. The idea is to identify a discriminative function or classifier with the largest potential generalization capacity that is known as predictive quality [20].

Frequently, SVMs depend on "kernels" to get around this. By projecting the data into a feature space – a vector space of higher dimension – or by bringing them back to the twodimensional space, these mathematical functions enable the separation of the data [40]. The nonlinear decision boundary was explained by a kernel function K (equation (2)) [39].

$$K(\vec{x_i}, \vec{x_i}) = \emptyset(\vec{x_i})^T \emptyset(\vec{x_i}). \tag{2}$$

The function \emptyset was used to map the training vector $(\vec{x_i})$ into a high-dimensional space. To deal with nonlinear problems, three kernel functions were regularly introduced. This study used three types of kernel functions listed below: the linear kernel function (equation (3)), radial basis kernel function (equation (4)), and polynomial kernel function (equation (5)). Using geographic information system (GIS) methods, the environmental parameters were determined.

$$K(\overrightarrow{x_i}, \overrightarrow{x_i}) = \overrightarrow{x_i}^T \times \overrightarrow{x_i}, \tag{3}$$

$$K(\vec{x_i}, \vec{x_i}) = \exp\{-/\delta^2 ||\vec{x_i} - \vec{x_i}||^2\},$$
 (4)

where δ^2 is the radial basis function's bandwidth.

$$K(\overrightarrow{x_i}, \overrightarrow{x_i}) = (yX_i^T + r)^d, \tag{5}$$

when y > 0, the polynomial kernel has degree d.

2.3 Landslide inventory, risk variables, and data sources

For this investigation, the following were the main sources of data: (1) published survey data and landslide reports, (2) Landsat 8 remote sensing images, (3) a 15 m resolution digital elevation model (DEM), and (4) topographic and geology maps at a scale of 1:50,000.

2.3.1 Landslide inventory

Using a geology inventory to find and classify landslides is a helpful method for LSM. Precise mapping of landslide susceptibility was established by gathering pertinent reports

and photos, as well as by carrying out a survey at a 1:50,000 scale. There have been numerous recorded landslides in the area, including rock blades, debris flows, and debris avalanches. In the present study, the landslide dataset comprises a total of 200 documented landslide events within the Oued Aoulai watershed, with 140 landslides used for model training and 60 for validation. The dataset includes various types of landslides, such as debris flows, rockfalls, and translational slides, which are prevalent in the region. Key characteristics of the landslides include their geographical distribution, with occurrences primarily concentrated in steep slopes and areas with specific geological formations. This diverse dataset allows for a comprehensive evaluation of the models' performance and enhances the reliability of the susceptibility mapping. This study used the fieldwork, data from satellite image analysis, and historical records to create a map of active landslides. In this way, a list of almost 1,000 landslides in the research region was generated.

2.3.2 Landslide causative factors

The factors considered for LSM in the Oued Aoulai watershed were briefly outlined by using in-depth literature review, brainstorming, and discussion with experts. The data sources for these factors include satellite imagery for land cover classification, topographic maps for slope analysis, and geological surveys for understanding subsurface conditions. The factors were processed using GIS software, which facilitated spatial analysis and integration of various datasets, alongside statistical analysis tools for correlation and sensitivity assessments. This streamlined approach ensures that the factors are relevant and effectively contribute to the susceptibility mapping process.

The features of the research area guided the subjective selection of landslide-causing elements [41]. The topographic position index (TPI), topographic wetness index (TWI), lithology, distance from faults, slope gradient, slope aspect, soil texture, curvature, precipitation, land use and land cover (LULC), distance from highways, and normalized difference vegetation index (NDVI) were among the 14 landslide-causing components that were investigated in this study. The selection of these factors was based on expert judgment, a review of the literature, and the availability of data at the appropriate scale by referring to successful research outcomes from the published literature such as Sachdeva et al. and Bashir et al. [42,43]. Slope inclination - landslides occur more frequently on hillside slopes that are steeper [44]. Since the slope gradient affects the soil moisture content and is required for subsurface flow [45], this has a direct bearing on how frequently landslides occur.

NDVI is recognized as an important variable in landslide susceptibility modeling, even though it significantly enhances the cohesiveness and shear strength of lithologic mass and immobilizes vast amounts of water [44,46]. Using the January 2023 images, equation (6) was applied to determine the present research region's NDVI value.

$$NDVI = (NIR - R)/(NIR + R),$$
 (6)

where the electromagnetic spectrum's red band is denoted by R and the near-infrared band is represented by NIR.

Elevation is a topographical feature that affects how unstable slopes are. Almost all landslide susceptibility evaluations employ it often [47]. In terms of LULC, landslides are mostly caused in the study area by anthropogenic activities such as infrastructure development and urbanization. Roads and structures must be constructed because of these activities, which may alter the stability of the slope and the original geological conditions [48,49]. Earlier models included data on land use and cover [50–52] to assess vulnerability to natural disasters such as avalanches, flooding, wildfires, and landslides.

Soil texture describes each soil profile's materials and physical properties, with soil texture data taken from laboratory analyses. Tectonic deformations that might result in landslides are defined as weak spots in the rock, characterized by a drop in resistivity and can be brittle (faults, shears, etc.) or ductile folds [53–55]. Thus, the elimination of faults may serve as a warning indicator for landslides. The runoff from rivers contributes significantly to undercutting phenomena that increase the pore water pressure in the vicinity and trigger landslides [56]. As such, it has a major impact on the susceptibility to landslides [57].

One essential terrain variable used in many different kinds of geomorphometric research is curvature [58]. There are two types of curvatures: plane curvature and profile curvature. It is well established that the profile curvature controls these materials' downslope acceleration and deceleration to affect material deposition, while surface runoff's convergence and dispersion are directly impacted by plane curvature [59].

The TPI is the difference between a single cell's height and the average height of its neighbors [60,61]. The TWI is one of the characteristics that demonstrates the hydrological process linked to the build-up of water flow based on the regulation of the slope factor in a region [62]. Slope affects the hydrological cycle in observable ways in locations with high relief.

In terms of Aspect, the slope gradient can affect landslides both directly and indirectly in several processes, including the orientation of discontinuities, wind and precipitation patterns, soil moisture concentration, root development evapotranspiration, hydrological processes, vegetation, and solar radiation [63].

One of the significant anthropogenic activities that alters the morphology of natural slopes is the road building. This changes how close the slopes are to roads and forecasts the intensity of the landslides [64]. Precipitation data can be used to calculate the amount of water that accumulates and causes landslides, as well as the movement of materials and soil [65]. Lithology is important to LMS and influences various types of landslides. Numerous mechanical and physical properties, including the kind, degree of weathering resistance, density, durability, and permeability, are present in these units [66].

3 Results and discussion

3.1 Factors contributing to landslides

Building upon established techniques in the field, such as those demonstrated by [61] in their LR model case study, our approach integrates multiple ML models, including SVMs and RF. These methodologies are supported by recent findings in the literature [62], which highlight the efficacy of ML techniques in accurately predicting landslide susceptibility based on environmental factors.

Slope inclination: The slope map (Figure 3a) for this inquiry was created using the DEM and ranged from 0 to 55. The map was constructed at a resolution of 12 m.

NDVI: The current research region's NDVI values range from -0.13 to 0.67, where a positive number implies vegetated regions and a negative one denotes the barren land (Figure 3b).

Elevation: The elevation map in this study was made in accordance with the DEM's classification. It was situated above the sea level at a height of 198–1,583 m (Figure 3c).

LULC: The land use map used in this study was derived from the "Sentinel-2 10-Meter LULC" dataset. Six distinct land use types were identified in the research region: trees, water, crops, cultivated land, bare soil, and grassland (Figure 3d).

Soil type: The research region had an average soil composition of 18% sand, 32% silt, and 50% clay. Figure 3e illustrates the distribution of soil texture in the research region.

Distance from faults: Using GIS software, Euclidean Distance tool, a map was created, and the distance to faults was plotted. The 1:50,000 scale geology maps of the

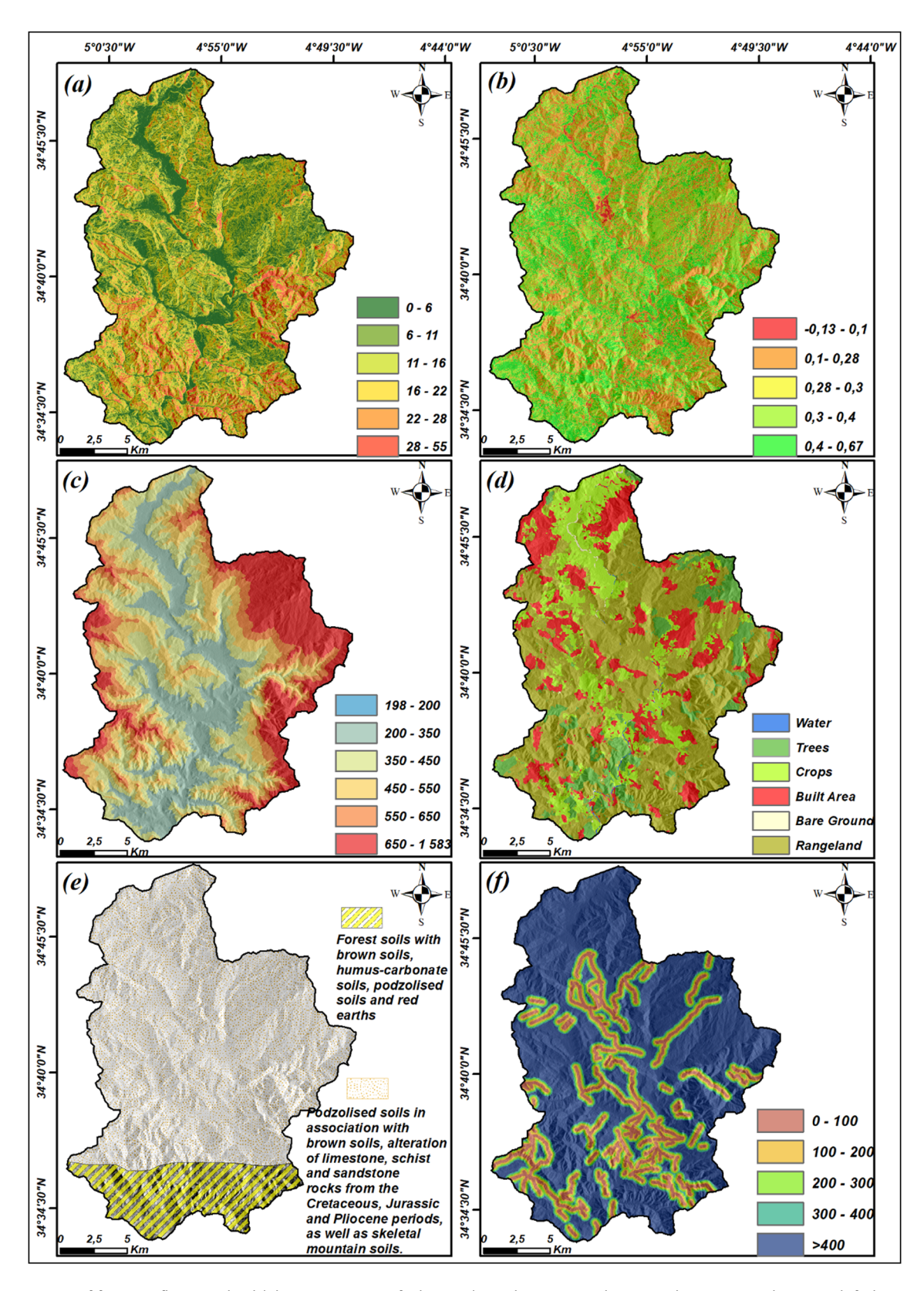


Figure 3: Maps of factors influencing landslide occurrence: DT faults, (a) slope, (b) NDVI, (c) elevation, (d) LULC, (e) soil type, and (f) distance from faults.

research area provided the faults employed in this investigation (Figure 3f). There could be anywhere from 0 to 400 m between faults.

Distance from rivers: The hydrographic network for this study was created using a DEM with a resolution of 12 m. The Euclidean distance approach in GIS software was used to derive the river's distance, which spans from 0 to 500 m.

Curvature: The plane and profile curvatures were derived from the DEM using GIS software. In the study area, the profile curvature exhibits a convex, flat shape, with values ranging from -4.43 to 4.66. Convex curvatures indicate a decelerating flow, while concave curvatures indicate an accelerating flow. The area's plane curvature often depicts the flow's convergence and divergence along a surface since it is perpendicular to the direction of the sharpest gradient. The three plane curvatures of the research region are concave, convex, and flat, and they range from -4.39 to 4.64 (Figure 4a).

TPI: Topographic landforms like valleys, slopes, and ridges can be identified by applying particular thresholds to the TPI values. Because hills are the source of most landslide ruts, the TPI may be utilized to produce a landslide susceptibility map. The TPI for the study area spans from –25.95 to 32.01 (Figure 4b).

TWI: The terrain wetness index highlights the significant influence of topography and soil moisture content on landslide probability. The research area's TWI (Figure 4c) varies from 2.41 to 21.6.

Aspect: The slope gradient in the research area was utilized to generate nine categories using the DEM: flat (1), north, northeast, east, southeast, south, southeast, west, and northeast (Figure 4e).

Distance from roads: The elimination of highways could be a sign that landslides are about to happen. In the current experiment, the range of highway distances (0–500 m) was generated using the Euclidean distance tool within the GIS software (Figure 4f).

Rainfall: The rainfall condition map is illustrated in Figure 5a, and Figure 5b shows the geographical distribution of average precipitation data over 10 years.

Lithology: The Moroccan Ministry of Mines and Geology provided two geological maps (scale, 1/50,000) from which the lithology used in this study was derived; Rhafsay-kelaa des sles and Tafrannt de l'Ouerra-Moulay Bouchta (Figure 5b).

3.2 Multicollinearity analysis

Determining the multicollinearity of land cover factors (LCFs) is essential in any multivariable landslide simulation.

The extent to which independent variables are interdependent can significantly impact a model's overall accuracy. Excessive multicollinearity, for example, may reduce the predictive power of the model, emphasizing the need for rigorous assessment to ensure the stability and reliability of simulation results [67,68].

The 14 components' multicollinearity was tested using variance inflation factors (VIFs) and tolerances. Multicollinearity is defined as a tolerance of less than 0.2 or a VIF of 5.0 or more [63,64]. These thresholds are commonly used in statistical analysis to identify potential multicollinearity issues among predictor variables. A tolerance value below 0.2 indicates that the variable shares a significant amount of variance with other predictors, which can lead to unreliable coefficient estimates and inflated standard errors. Similarly, a VIF exceeding 5.0 suggests that the variable is highly correlated with one or more other predictors, warranting further investigation to ensure the stability and reliability of the model. Investigation of the conditioning variables indicates that every landslide conditioning variable utilized in the LSM for this case study is trustworthy and safe to apply (Table 1).

The result demonstrates that the lowest TOL value is somewhat greater. Elevation reaches the maximum VIF of 2.147012 and the lowest TOL of 0.46576, indicating that the maximum VIF is likewise far below the cutoff level.

3.3 Pearson correlation coefficient

The Pearson correlation coefficient, abbreviated "r," is a popular statistical metric for determining the direction and strength of a linear relationship between two variables. Equation (7) defines how to calculate this coefficient and gives a numerical representation of the degree of linear relationship between the two parameters:

$$\rho_{x,y} = \frac{\operatorname{Cov}(x,y)}{\sigma_x \sigma_y} = \frac{[(x - \mu_x)(y - \mu_y)]}{\sigma_x \sigma_y},\tag{7}$$

where

- Cov(x,y) represents the covariance of x and y between two elements; σ_x and σ_y represent the standard deviations of x and y, respectively, and μ_x and μ_y represent the means of x and y, respectively.

Equation (3) depicts the mathematical expectation. A Pearson correlation coefficient absolute value greater than 0.5 often indicates a significant link between the two parameters [68,69]. The correlation coefficient matrix of this study reveals no strong correlations among the 14 conditioning factors, indicating that no conditioning factors need to be eliminated (Figure 6).

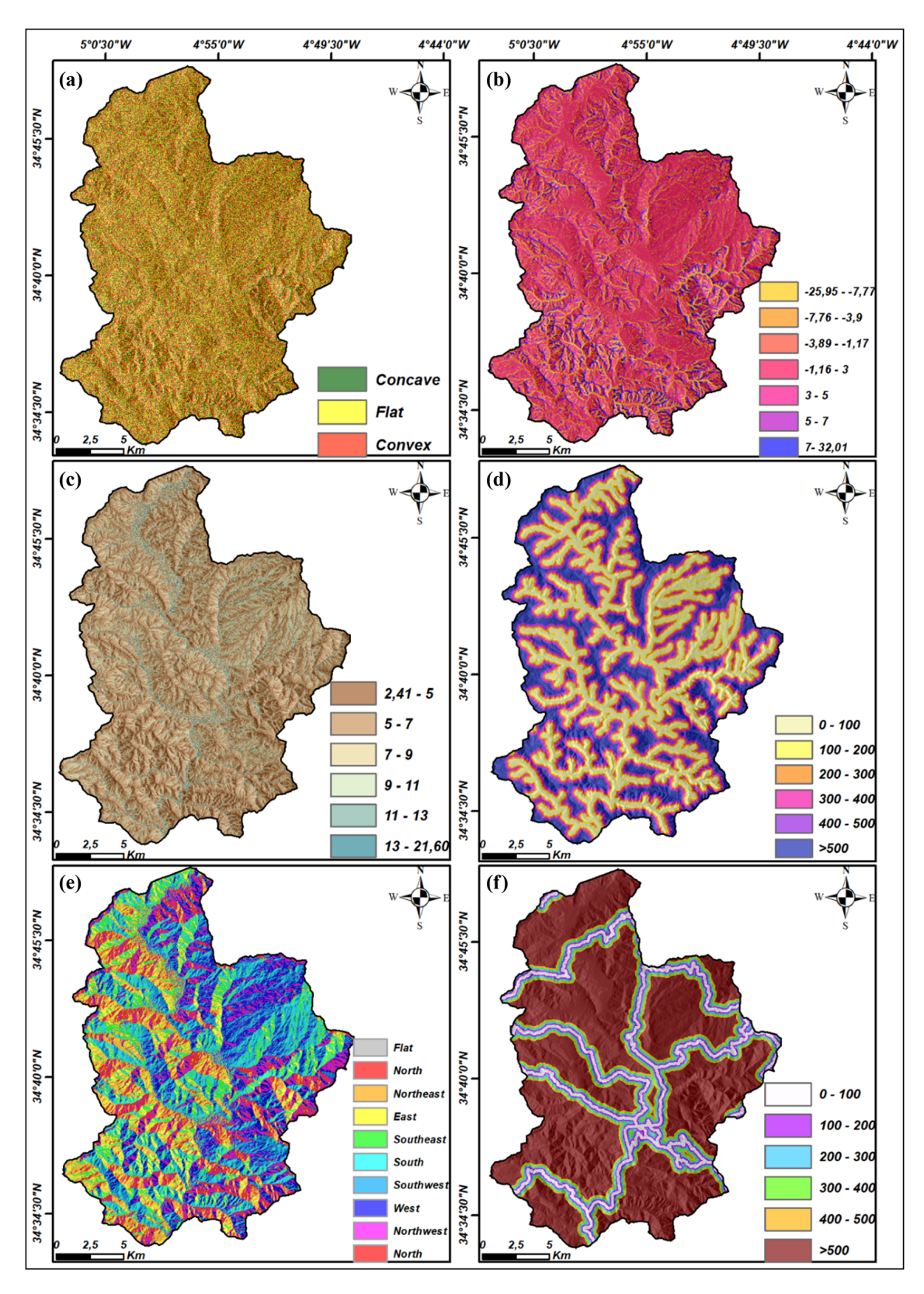


Figure 4: Maps of the landslide conditioning factor: (a) curvature, (b) TPI, (c) TWI, (d) Distance from river, (e) aspect, and (f) DT roads.

10 — Latifa Ladel et al. DE GRUYTER

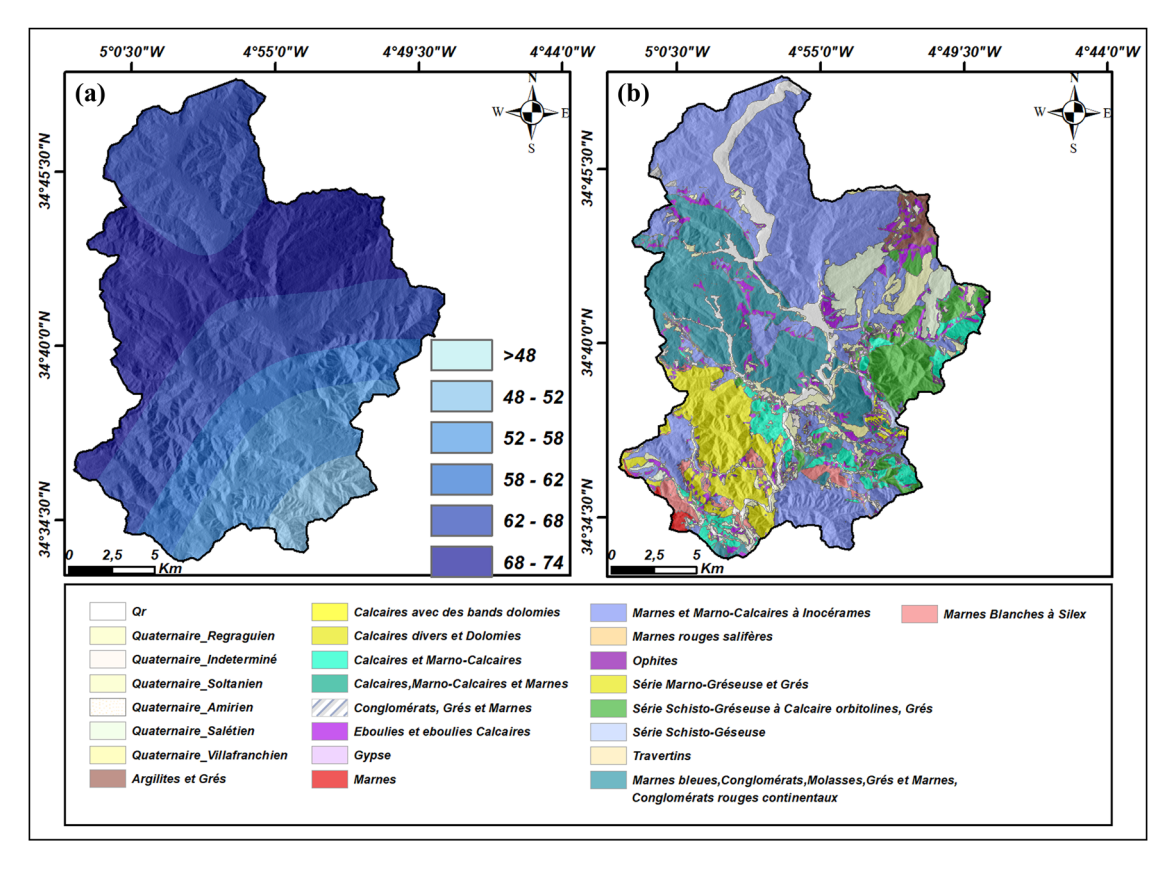


Figure 5: Landslide conditioning factor maps: (a) rainfall and (b) lithology.

Table 1: Multicollinearity diagnosis results

Variable	VIF	Tolerance		
variable	VIF			
Curvature	2.147012	0.46576		
DT rivers	2.095214	0.47728		
DT roads	1.816736	0.55044		
Slope	1.47478	0.67807		
DT faults	1.461652	0.68416		
Aspect	1.461243	0.68435		
Rainfall	1.440201	0.69435		
TWI	1.31355	0.7613		
TPI	1.280253	0.7811		
Soil type	1.240115	0.80638		
Lithology	1.213983	0.82373		
DEM	1.181745	0.84621		
NDVI	1.161018	0.86131		
LULC	1.146891	0.87192		

3.4 Mapping the susceptibility of landslides

Figure 7 compares two landslide susceptibility maps created with RF and SVM models. From extremely low to extremely high susceptibility classifications, five were identified (Figure 8). Specific vulnerable zones were

identified using the outcomes of each landslide susceptibility model. The proportional percentages of the area that each vulnerability class was assigned in the models were carefully selected to give thorough information and enhance the comparison analysis's granularity.

3.5 Model performance and validation

The current study used a variety of statistical and graphical performance measures to assess the prediction performance of the SVM and RF models. For classification problems, the confusion matrix was frequently utilized. False positive (FP), false negative (TN), true positive (TP), and false negative (FN) values were used to identify counts of genuine and predicted values. TP stands for the number of properly categorized genuine landslide pixels, TN for accurately classified non-landslide pixels, FP for accurately classified actual landslide pixels, and FN for accurately classified actual landslide pixels. The following calculations were performed: accuracy, precision, recall, confusion matrix, mean absolute error (MAE), and root mean square error (RMSE).

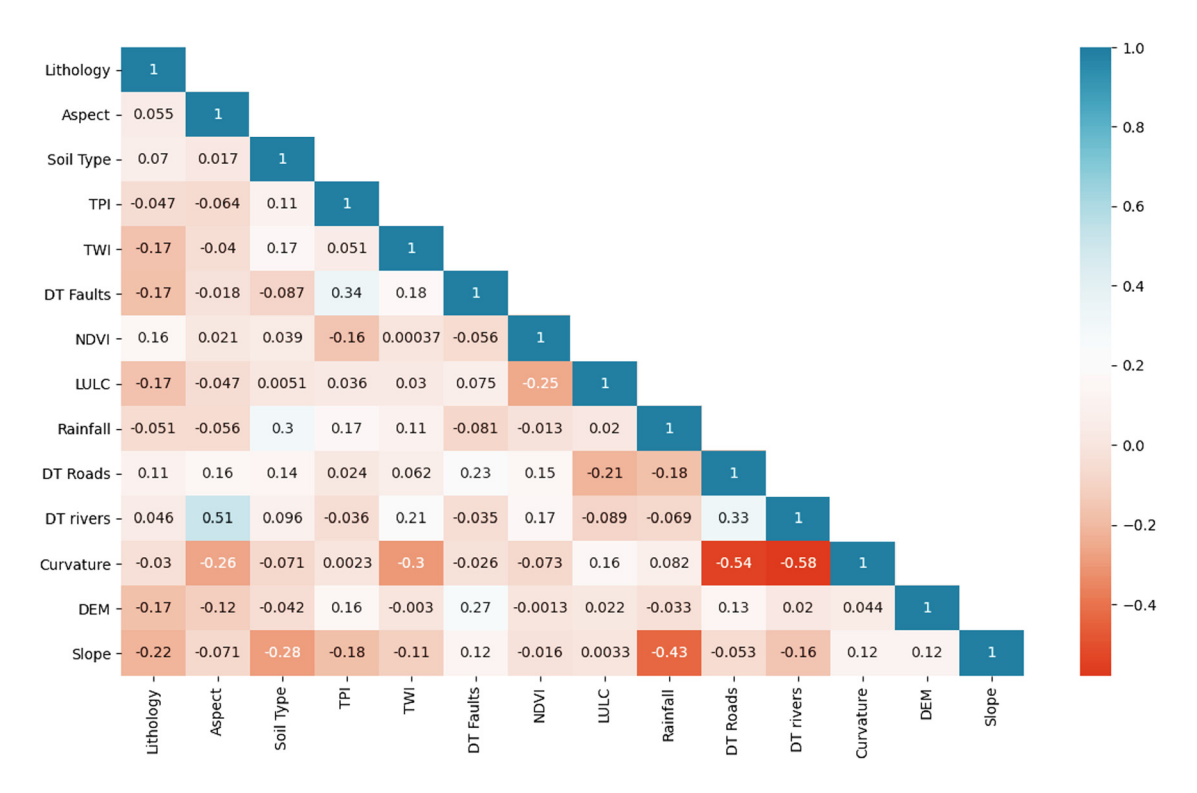


Figure 6: Matrix with Pearson correlation coefficients for various elements.

AUC values from receiver operating characteristic (ROC) curves are often used to calculate the classification performance. The AUC is particularly valuable in the context

of imbalanced data, as it provides a single metric that captures the model's ability to differentiate between classes, regardless of their distribution. This is crucial in landslide

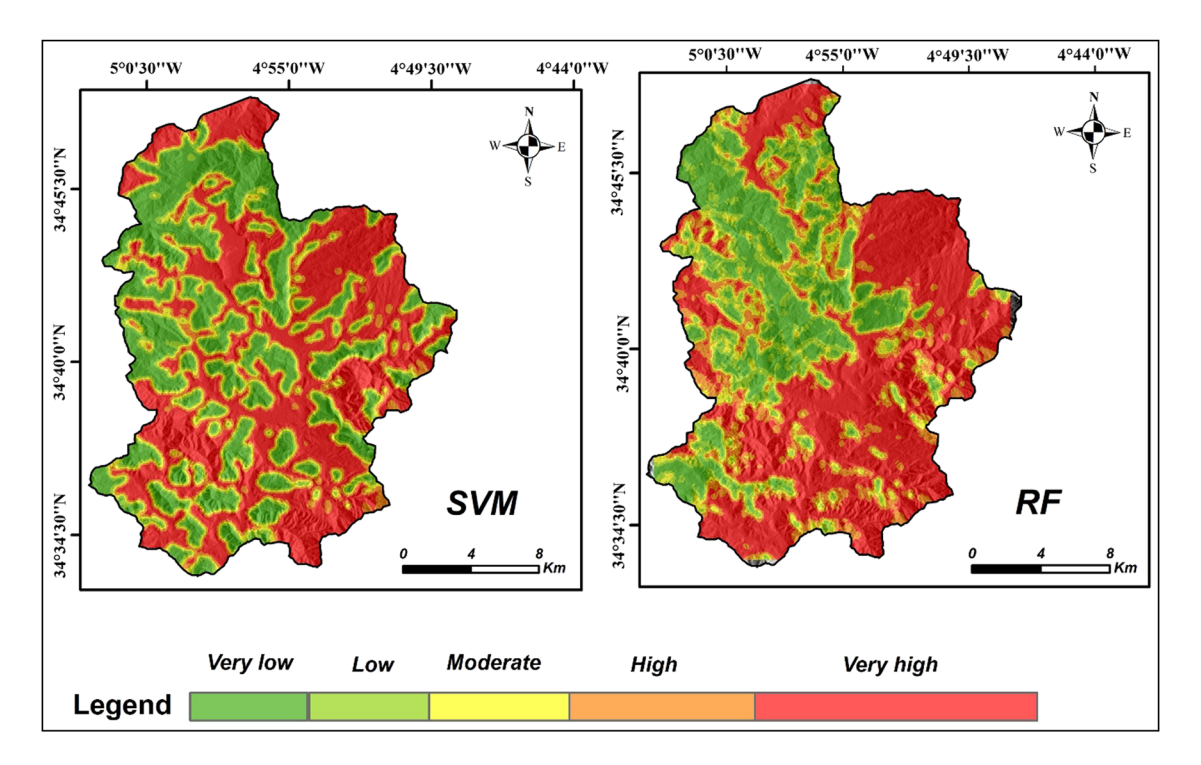


Figure 7: Generated landslide susceptibility maps using the SVM and RF.

12 — Latifa Ladel et al. DE GRUYTER

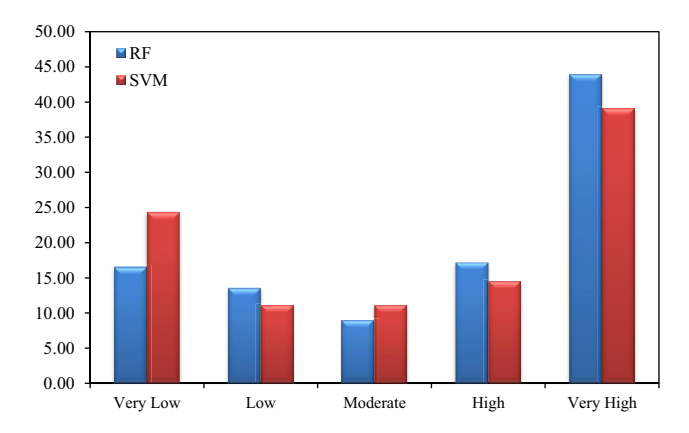


Figure 8: Area % for landslide susceptibility classes using the applied MLTs.

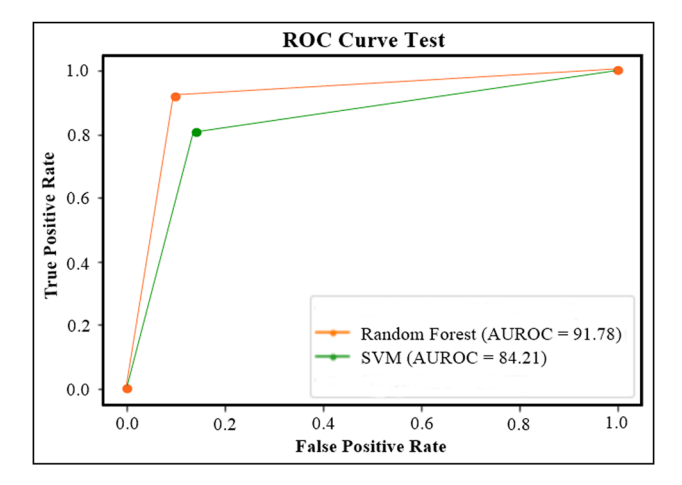


Figure 9: Implemented model's stacked ROC curves.

susceptibility modeling, where the number of susceptible versus non-susceptible locations may not be evenly distributed. A higher AUC indicates better model performance across all classification thresholds [70,71], making it a preferred metric for evaluating the efficacy of our models. The greater the AUC score, the better the model forecasts landslides and non-landslides. The AUC prediction curve was generated using the landslide inventory training dataset, while the AUC validation curve and performance matrices were created using the validation dataset.

Figure 9 displays the training accuracies of the SE-FR and SE-SVM models, which were 94.7 and 80.65 AUC, respectively. According to the confusion matrices, the SE-FR and SE-SVM models have 0.946 and 0.906 accuracy, 0.904 and 0.863 precision, and 0.982 and 0.902 recall, respectively. Table 2 displays the MAE and RMSE values for the SE-FR and SE-SVM models, which were 0.053 and 0.193, 0.230 and 0.439, respectively. According to the studies of Youssef et al., Aguirre-Gutiérrez et al., and Sestras et al. [8,72,73], evaluating a model's performance using a single metric, such as AUC, is not necessarily meaningful, because high AUC does not always imply a high degree of accuracy in spatial predictions.

Both models exhibit good prediction, recall, and accuracy scores, and their respective MAE and RMSE errors fall within acceptable bounds, according to the prediction matrix results. These statistical and visual performance measures show that both models have respectable error values and a strong potential for prediction. As a result, it was discovered that RF performed better than the SVM model when utilizing the AUC technique. However, when the RMSE technique was used, the SVM fared better than the RF model.

4 Conclusions

LSM is a crucial geomatic technique for effective risk assessment and watershed management because different regions of Morocco are always at risk due to factors such as lithology, climate, geology, land use/cover, vegetation, anthropogenic interventions, and other related factors. The current study employed two ML models to evaluate the specified region in terms of landslide scenarios: SVM and RF. This was done since creating viable and realistic susceptibility maps is essential for preventive actions and treatments. According to the thorough investigation and analytical approach, the RF model classified 30.07% of the research region as low susceptible to landslides, 8.88% as moderately susceptible, and 61.06% as extremely susceptible. On the other hand, the SVM model determined that 35.41% of the region was susceptible to landslides at a low level, 11.08% at a moderate level, and 53.5% at a high level.

Table 2: Models' RMSE and AUC

	Performance indicators	Precision	Accuracy	Recall	MAE	RMSE	AUC
Model	RF	0.904	0.946	0.982	0.053	0.230	94.7
	SVM	0.863	0.906	0.902	0.193	0.439	80.65

The performance of the models was tested using the AUC and RMSE measurements, and the results were favorable. The RF model had an AUC of 94.7%, while the SVM model had an AUC of 80.65%. In the end, the RF and SVM models provide strong and trustworthy findings for mapping the susceptibility of landslides. Since the resulting hazard mapping scenarios give crucial information for informed watershed planning and development strategies, they are of great value to local authorities.

Funding information: No funding was received for this research.

Author contributions: Latifa Ladel and Mohamed Mastere - conceived and designed the studies; Latifa Ladel, Mohamed Mastere, Shuraik Kader, Velibor Spalević, and Branislav Dudic - performed the analysis; Latifa Ladel, Mohamed Mastere, Shuraik Kader, Velibor Spalević, and Branislav Dudic – analyzed and interpreted the data; Latifa Ladel, Mohamed Mastere, Shuraik Kader, Velibor Spalević, and Branislav Dudic - contributed materials, analysis tools, or data; Latifa Ladel, Mohamed Mastere, Shuraik Kader, Velibor Spalević, and Branislav Dudic - preparation of draft; Mohamed Mastere, Shuraik Kader, and Velibor Spalević – internal reviewers; Mohamed Mastere – project administration. All authors have read and agreed to the submitted version of the manuscript.

Conflict of interest: The authors have no relevant financial or non-financial interests to disclose.

Ethical approval: Not Applicable.

Consent to participate: Not Applicable.

Consent to publish: Not Applicable.

Data availability statement: The data and materials will be available on request.

References

- Benzougagh B, Meshram SG, Baamar B, Dridri A, Boudad L, Sadkaoui D, et al. Relationship between landslide and morphostructural analysis: A case study in Northeast of Morocco. Appl Water Sci. 2020;10(7):1-10. doi: 10.1007/s13201-020-01258-4.
- Fan X, Scaringi G, Korup O, West AJ, van Westen CJ, Tanyas H, et al. Earthquake-induced chains of geologic hazards: Patterns, mechanisms, and impacts. Rev Geophysics. 2019;57(2):421-503. doi: 10.1029/2018RG000626.

- Zejak D, Spalević V, Popović V, Markoski M, Dudić B, Ouallali A, et al. Analysis of the presence of heavy metals in the soils of the hillymountainous areas of Balkan Peninsula with the assessment of its potential for the fruit growing: Case study of the Ljubovidja river basin, Polimlje, Montenegro. In Proceedings, 26 International Eco-Conference and 12 Safe Food, Novi Sad, 21-23 September 2022. Novi Sad: Ecological Movement of Novi Sad; 2022.
- [4] Guzzetti F. Mondini AC. Cardinali M. Fiorucci F. Santangelo M. Chang KT. Landslide inventory maps: New tools for an old problem. Earth-Sci Rev. 2012;112(1):42-66. doi: 10.1016/j.earscirev.2012.02.001.
- [5] Li Y, Liu X, Han Z, Dou J. Spatial proximity-based geographically weighted regression model for landslide susceptibility assessment: a case study of Qingchuan area, China. Appl Sci. 2020;10(3):1107. doi: 10.3390/app10031107.
- Bartholdson S, von Schreeb J. Natural disasters and injuries: What does a surgeon need to know? Curr Trauma Rep. 2018;4:103-8. doi: 10.1007/s40719-018-0125-3.
- Sadkaoui D, Brahim B, Kader S, Agharroud K, Mihraje AI, Aluni K, et al. Evaluation of tectonic activity using morphometric indices: Study of the case of Taïliloute ridge (middle-Atlas region, Morocco). J Afr Earth Sci. 2024;213:105219. doi: 10.1016/j.jafrearsci.2024.105219.
- Youssef B, Bouskri I, Brahim B, Kader S, Brahim I, Abdelkrim B, [8] et al. The contribution of the frequency ratio model and the prediction rate for the analysis of landslide risk in the Tizi N'tichka area on the national road (RN9) linking Marrakech and Ouarzazate. Catena. 2023;232:107464. doi: 10.1016/j.catena.2023.107464.
- [9] Ouallali A, Kader S, Bammou Y, Aqnouy M, Courba S, Beroho M, et al. Assessment of the erosion and outflow intensity in the rif region under different land use and land cover scenarios. Land. 2024;13:141. doi: 10.3390/land13020141.
- Γ101 Casagli N, Intrieri E, Carlà T, Di Traglia F, Frodella W, Gigli G, et al. Monitoring and early warning systems: Applications and perspectives. Understanding and reducing landslide disaster risk: Volume 3 Monitoring and Early Warning 5th. United Kingdom: Elsevier; 2021. p. 1-21. doi: 10.1007/978-3-030-60311-3_1.
- [11] Bammou Y, Benzougagh B, Abdessalam O, Brahim I, Kader S, Spalevic V, et al. Machine learning models for gully erosion susceptibility assessment in the Tensift catchment, Haouz Plain, Morocco for sustainable development. I Afr Earth Sci. 2024;213:105229. doi: 10.1016/j.jafrearsci.2024.105229.
- [12] Bammou Y, Benzougagh B, Igmoullan B, Ouallali A, Kader S, Spalevic V, et al. Optimizing flood susceptibility assessment in semi-arid regions using ensemble algorithms: A case study of Moroccan High Atlas. Nat Hazards. 2024;120:7787-816. doi: 10.1007/s11069-024-06550-z.
- Corominas J, van Westen C, Frattini P, Cascini L, Malet JP, Fotopoulou S, et al. Recommendations for the quantitative analysis of landslide risk. Bull Eng Geol Environ. 2014;73:209-63. doi: 10. 1007/s10064-013-0538-8.
- Nwazelibe VE, Unigwe CO, Egbueri JC. Testing the performances of different fuzzy overlay methods in GIS-based landslide susceptibility mapping of Udi Province, SE Nigeria. Catena. 2023;220:106654. doi: 10.1016/j.catena.2022.106654.
- Aghdam IN, Varzandeh MHM, Pradhan B. Landslide susceptibility mapping using an ensemble statistical index (Wi) and adaptive neuro-fuzzy inference system (ANFIS) model at Alborz Mountains (Iran). Environ Earth Sci. 2016;75:1-20. doi: 10.1007/s12665-015-
- [16] Wang L-I, Sawada K, Moriguchi S. Landslide susceptibility analysis with logistic regression model based on FCM sampling strategy. Computers Geosci. 2013;57:81-92. doi: 10.1016/j.cageo.2013.04.006.

- [17] Bashir O, Bangroo SA, Shafai SS, Senesi N, Naikoo NB, Kader S, et al. Unlocking the potential of soil potassium: Geostatistical approaches for understanding spatial variations in Northwestern Himalayas. Ecol Inform. 2024;81:102592. doi: 10.1016/j.ecoinf.2024. 102592
- [18] San BT. An evaluation of SVM using polygon-based random sampling in landslide susceptibility mapping: The Candir catchment area (western Antalya, Turkey). Int J Appl Earth Geoinf. 2014;26:399–412. doi: 10.1016/j.jag.2013.09.010.
- [19] Chang Z, Du Z, Zhang F, Huang F, Chen J, Li W, et al. Landslide susceptibility prediction based on remote sensing images and GIS: Comparisons of supervised and unsupervised machine learning models. Remote Sens. 2020;12(3):502. doi: 10.3390/rs12030502.
- [20] Benzougagh B, Meshram SG, Fellah BE, Mastere M, El Basri M, Ouchen I, et al. Mapping of land degradation using spectral angle mapper approach (SAM): the case of Inaouene watershed (Northeast Morocco). Modeling Earth Syst Environ. 2023;10:1–11. doi: 10.1007/s40808-023-01711-8.
- [21] Pourghasemi HR, Rahmati O. Prediction of the landslide susceptibility: Which algorithm, which precision? Catena. 2018;162:177–92. doi: 10.1016/j.catena.2017.11.022.
- [22] Hu X, Wu S, Zhang G, Zheng W, Liu C, He C, et al. Landslide displacement prediction using kinematics-based random forests method: A case study in Jinping Reservoir Area, China. Eng Geol. 2021;283:105975. doi: 10.1016/j.enggeo.2020.105975.
- [23] Bashir O, Bangroo SA, Shafai SS, Senesi N, Kader S, Alamri S. Geostatistical modeling approach for studying total soil nitrogen and phosphorus under various land uses of North-Western Himalayas. Ecol Inform. 2024;80:102520. doi: 10.1016/j.ecoinf.2024. 102520.
- [24] Guo C, Montgomery DR, Zhang Y, Wang K, Yang Z. Quantitative assessment of landslide susceptibility along the Xianshuihe fault zone, Tibetan Plateau, China. Geomorphology. 2015;248:93–110. doi: 10.1016/j.geomorph.2015.07.012.
- [25] Loudyi D, Hasnaoui MD, Fekri A. Flood risk management practices in Morocco: Facts and challenges. Wadi Flash Floods. 2022;35:35–94.
- [26] Sahrane R, El Kharim Y, Bounab A. Investigating the effects of landscape characteristics on landslide susceptibility and frequencyarea distributions: The case of Taounate province, Northern Morocco. Geocarto Int. 2022;37(27):17686–712. doi: 10.1080/ 10106049.2022.2134462.
- [27] Sahrane R, Bounab A, El Kharim Y. Investigating the effects of landslides inventory completeness on susceptibility mapping and frequency-area distributions: Case of Taounate province, Northern Morocco. Catena. 2023;220:106737. doi: 10.1016/j.catena.2022. 106737.
- [28] Sahrane R, Bounab A, Obda I, Obda O, El Hamdouni R, EL Kharim Y. Assessing the reliability of landslides susceptibility models with limited data: Impact of geomorphological diversity and technique selection on model performance in Taounate Province, Northern Morocco. Earth Syst Environ. 2024;9:1–25. doi: 10.1007/s41748-024-00455-4
- [29] Leblanc D, Olivier P. Role of strike-slip faults in the Betic-Rifian orogeny. Tectonophysics. 1984;101(3):345–55. doi: 10.1016/0040-1951(84)90120-3.
- [30] Bahrouni N, Masson F, Meghraoui M, Saleh M, Maamri R, Dhaha F, et al. Active tectonics and GPS data analysis of the Maghrebian thrust belt and Africa-Eurasia plate convergence in Tunisia. Tectonophysics. 2020;785:228440. doi: 10.1016/j.tecto.2020.228440.

- [31] Ait Brahim L, Chotin P. Genèse et déformation des bassins néogènes du Rif central (Maroc) au cours du rapprochement Europe-Afrique. Geodinamica Acta. 1989;3(4):295–304. doi: 10. 1080/09853111.1989.11105194.
- [32] Liu R, Li L, Pirasteh S, Lai Z, Yang X, Shahabi H. The performance quality of LR, SVM, and RF for earthquake-induced landslides susceptibility mapping incorporating remote sensing imagery. Arab J Geosci. 2021;14:1–15. doi: 10.1007/s12517-021-06573-x.
- [33] Youssef AM, Pourghasemi HR, Pourtaghi ZS, Al-Katheeri MM. Landslide susceptibility mapping using random forest, boosted regression tree, classification and regression tree, and general linear models and comparison of their performance at Wadi Tayyah Basin, Asir Region, Saudi Arabia. Landslides. 2016:13:839–56. doi: 10.1007/s10346-015-0614-1.
- [34] Xu K, Zhao Z, Chen W, Ma J, Liu F, Zhang Y, et al. Comparative study on landslide susceptibility mapping based on different ratios of training samples and testing samples by using RF and FR-RF models. Nat Hazards Res. 2023;20:273–97. doi: 10.1016/j.nhres. 2023.07.004.
- [35] Breiman L. Random forests. Mach Learn. 2001;45:5–32. doi: 10. 1023/A:1010933404324.
- [36] Darminto M, Chu H-J. Mapping landslide release area using random forest model. In IOP Conference Series: Earth and Environmental Science. United Kingdom: Elsevier; 2019. doi: 10. 1088/1755-1315/389/1/012038.
- [37] Youssef AM, Pradhan B, Tarabees E. Integrated evaluation of urban development suitability based on remote sensing and GIS techniques: contribution from the analytic hierarchy process. Arab J Geosci. 2011;4:463–73. doi: 10.1007/s12517-009-0118-1.
- [38] Merghadi A, Yunus AP, Dou J, Whiteley J, ThaiPham B, Bui DT, et al. Machine learning methods for landslide susceptibility studies: A comparative overview of algorithm performance. Earth-Sci Rev. 2020;207:103225. doi: 10.1016/j.earscirev.2020.103225.
- [39] Cortes C, Vapnik V. Support-vector networks. Mach Learn. 1995;20:273–97. doi: 10.1007/BF00994018.
- [40] Giovanis DG, Shields MD. Data-driven surrogates for high dimensional models using Gaussian process regression on the Grassmann manifold. Computer Methods Appl Mech Eng. 2020;370:113269. doi: 10.1016/j.cma.2020.113269.
- [41] Zhou C, Yin K, Cao Y, Ahmed B, Li Y, Catani F, et al. Landslide susceptibility modeling applying machine learning methods: A case study from Longju in the Three Gorges Reservoir area, China. Computers Geosci. 2018;112:23–37. doi: 10.1016/j.cageo.2017.11.019.
- [42] Sachdeva S, Bhatia T, Verma AK. A novel voting ensemble model for spatial prediction of landslides using GIS. Int J Remote Sens. 2020;41(3):929–52. doi: 10.1080/01431161.2019.1654141.
- [43] Bashir O, Bangroo SA, Shafai SS, Shah TI, Kader S, Jaufer L, et al. Mathematical vs. machine learning models for particle size distribution in fragile soils of North-Western Himalayas. J Soils Sediment. 2024;13(3):385. doi: 10.1007/s11368-024-03820-y.
- [44] Youssef AM, Pourghasemi HR. Landslide susceptibility mapping using machine learning algorithms and comparison of their performance at Abha Basin, Asir Region, Saudi Arabia. Geosci Front. 2021;12(2):639–55. doi: 10.1016/j.gsf.2020.05.010.
- [45] Magliulo P, Di Lisio A, Russo F, Zelano A. Geomorphology and landslide susceptibility assessment using GIS and bivariate statistics: A case study in southern Italy. Nat Hazards. 2008;47(3):411–35. doi: 10.1007/s11069-008-9230-x.
- [46] Riaz MT, Basharat M, Brunetti MT. Assessing the effectiveness of alternative landslide partitioning in machine learning methods

- for landslide prediction in the complex Himalayan terrain. Prog Phys Geogr: Earth Environ. 2023;47(3):315-47. doi: 10.1177/ 03091333221113660.
- [47] Feizizadeh B, Blaschke T, Nazmfar H. GIS-based ordered weighted averaging and Dempster-Shafer methods for landslide susceptibility mapping in the Urmia Lake Basin, Iran. Int J Digital Earth. 2014;7(8):688-708. doi: 10.1080/17538947.2012.749950.
- [48] Xiao T, Yin K, Yao T, Liu S. Spatial prediction of landslide susceptibility using GIS-based statistical and machine learning models in Wanzhou County, Three Gorges Reservoir, China. Acta Geochim. 2019;38:654-69. doi: 10.1007/s11631-019-00341-1.
- [49] Sestras P, Bilașco Ș, Roșca S, Dudic B, Hysa A, Spalević V. Geodetic and UAV monitoring in the sustainable management of shallow landslides and erosion of a susceptible urban environment. Remote Sens. 2021;13(3):385. doi: 10.3390/rs13030385.
- [50] Choubin B, Rahmati O, Soleimani F, Alilou H, Moradi E, Alamdari N. Regional groundwater potential analysis using classification and regression trees. In: Pourghasemi HR, Gokceoglu C, editors. Spatial modeling in GIS and R for earth and environmental sciences. United Kingdom: Elsevier; 2019. p. 485-98. doi: 10.1016/B978-0-12-815226-3.00022-3.
- [51] Hysa A, Spalevic V, Dudic B, Roșca S, Kuriqi A, Bilașco Ş, et al. Utilizing the available open-source remotely sensed data in assessing the wildfire ignition and spread capacities of vegetated surfaces in Romania. Remote Sens. 2021;13(14):2737. doi: 10.3390/rs13142737.
- [52] Debnath J, Sahariah D, Nath N, Saikia A, Lahon D, Islam MN, et al. Modelling on assessment of flood risk susceptibility at the Jia Bharali River basin in Eastern Himalayas by integrating multicollinearity tests and geospatial techniques. Modeling Earth Syst Environ. 2023;139-140:1-27. doi: 10.1007/s40808-023-01912-1.
- [53] Lee S, Chwae U, Min K. Landslide susceptibility mapping by correlation between topography and geological structure: the Janghung area, Korea. Geomorphology. 2002;46(3):149-62. doi: 10. 1016/S0169-555X(02)00057-0.
- [54] Kanungo DP, Arora MK, Sarkar S, Gupta RP. A comparative study of conventional, ANN black box, fuzzy and combined neural and fuzzy weighting procedures for landslide susceptibility zonation in Darjeeling Himalayas. Eng Geol. 2006;85(3):347-66. doi: 10.1016/j. enggeo.2006.03.004.
- [55] Bucci F, Santangelo M, Cardinali M, Fiorucci F, Guzzetti F. Landslide distribution and size in response to Quaternary fault activity: the Peloritani Range, NE Sicily, Italy. Earth Surf Process Landf. 2016;41(5):711-20. doi: 10.1002/esp.3898.
- [56] Hadji R, Boumazbeur A, Limani Y, Baghem M, Chouabi AM, Demdoum A. Geologic, topographic and climatic controls in landslide hazard assessment using GIS modeling: A case study of Souk Ahras region, NE Algeria. Quat Int. 2013;302:224-37. doi: 10.1016/j. quaint.2012.11.027.
- [57] Pradhan B, Mansor S, Pirasteh S, Buchroithner MF. Landslide hazard and risk analyses at a landslide prone catchment area using statistical based geospatial model. Int J Remote Sens. 2011;32(14):4075-87. doi: 10.1080/01431161.2010.484433.
- Romstad B, Etzelmüller B. Mean-curvature watersheds: A simple method for segmentation of a digital elevation model into terrain units. Geomorphology. 2012;139-140:293-302. doi: 10.1016/j. geomorph.2011.10.031.
- [59] Prasicek G, Otto JC, Montgomery DR, Schrott L. Multi-scale curvature for automated identification of glaciated mountain landscapes. Geomorphology. 2014;209:53-65. doi: 10.1016/j.geomorph. 2013.11.026.

- [60] Mascandola C, Luzi L, Felicetta C, Pacor F. A GIS procedure for the topographic classification of Italy, according to the seismic code provisions. Soil Dyn Earthq Eng. 2021;148:106848. doi: 10.1016/j. soildyn.2021.106848.
- [61] Dahal MS, Chhetri A, Ghalley H, Pasang S, Patra M. Chapter 45 -Landslide susceptibility mapping along the Thimphu-Phuentsholing highway using machine learning. Pourghasemi HR, editor. Computers in earth and environmental sciences. Switzerland: MDPI: 2022. p. 601-17. doi: 10.1016/B978-0-323-89861-4.00038-5.
- [62] Wu Z, Baartman JEM, Pedro Nunes J, López-Vicente M. Intra-annual sediment dynamic assessment in the Wei River Basin, China, using the AIC functional-structural connectivity index. Ecol Indic. 2023;146:109775. doi: 10.1016/j.ecolind.2022.109775.
- [63] Quan H-C, Lee B-G. GIS-based landslide susceptibility mapping using analytic hierarchy process and artificial neural network in Jeju (Korea). KSCE J Civ Eng. 2012;16(7):1258-66. doi: 10.1007/ s12205-012-1242-0.
- [64] Kalantar B, Ueda N, Saeidi V, Janizadeh S, Shabani F, Ahmadi K, et al. Deep neural network utilizing remote sensing datasets for flood hazard susceptibility mapping in Brisbane, Australia. Remote Sens. 2021:13(13):2638.
- [65] Huo A, Yang L, Peng J, Cheng Y, Jiang C. Spatial characteristics of the rainfall induced landslides in the Chinese Loess Plateau. Hum Ecol Risk Assessment: An Int J. 2020;26(9):2462-77. doi: 10.1080/ 10807039.2020.1728517.
- Sun D, Ding Y, Zhang J, Wen H, Wang Y, Xu J, et al. Essential insights [66] into decision mechanism of landslide susceptibility mapping based on different machine learning models. Geocarto Int. 2022;51(3):1-29. doi: 10.1080/10106049.2022.2146763.
- [67] Arabameri A, Saha S, Roy J, Chen W, Blaschke T, Tien Bui D. Landslide susceptibility evaluation and management using different machine learning methods in the Gallicash River Watershed, Iran. Remote Sens. 2020;12(3):475. doi: 10.3390/rs12030475.
- Wang Y, Feng L, Li S, Ren F, Du Q. A hybrid model considering spatial heterogeneity for landslide susceptibility mapping in Zhejiang Province, China. Catena. 2020;188:104425. doi: 10.1016/j. catena.2019.104425.
- Bammou Y, Benzougagh B, Igmoullan B, Kader S, Ouallali A, Spalevic V, et al. Spatial mapping for multi-hazard land management in sparsely vegetated watersheds using machine learning algorithms. Environ Earth Sci. 2024;83(15):447. doi: 10.1007/s12665-024-11741-9.
- [70] Zhiyong F, Changdong L, Wenmin Y. Landslide susceptibility assessment through TrAdaBoost transfer learning models using two landslide inventories. Catena. 2023;222:106799. doi: 10.1016/j. catena.2022.106799.
- [71] Sbihi A, Mastere M, Benzougagh B, Spalevic V, Sestras P, Radovic M, et al. Assessing landslide susceptibility in northern Morocco: A geostatistical mapping approach in Al Hoceima-Ajdir. J Afr Earth Sci. 2024;218:105361. doi: 10.1016/j.jafrearsci.2024.105361.
- Aguirre-Gutiérrez J, Carvalheiro LG, Polce C, van Loon EE, Raes N, Reemer M, et al. Fit-for-purpose: species distribution model performance depends on evaluation criteria-Dutch hoverflies as a case study. PLoS One. 2013;8(5):e63708. doi: 10.1371/journal.pone.0063708.
- [73] Sestras P, Mircea S, Roșca S, Bilașco Ș, Sălăgean T, Dragomir LO, et al. GIS based soil erosion assessment using the USLE model for efficient land management: A case study in an area with diverse pedo-geomorphological and bioclimatic characteristics. Not Botanicae Horti Agrobotanici Cluj-Napoca. 2023;51(3):13263. doi: 10.15835/nbha51313263.